

Digital Texture Voxels for Stretchable Morphing Skin Applications

Caterina Lamuta,* Honglu He, Kaihao Zhang, Michael Rogalski, Nancy Sottos, and Sameh Tawfick*

The skin of the cephalopod is a 3D display, where the papillae muscles control the protrusion of each voxel by several millimeters out of the skin plane, create hierarchical textures, and collectively change the overall skin pattern in a fraction of a second. A material system capable of mimicking this response using electromechanical actuation of twisted spiral artificial muscles (TSAMs) is presented in this study. TSAMs leverage the mechanics of their twisted geometry to extend out of plane by 8 mm, corresponding to 2000% strain using a voltage of only 0.02 V mm^{-1} . They are made of polymer fibers wrapped with a helical metal wire. These actuators are assembled on a stretchable skin with the required flexible electrical connections to form an array of digital texture voxels (DTV). The DTV array produces arbitrary 3D surface patterns on-demand, and provides opportunities to control hydrodynamic drag, camouflage, and haptic displays.

Smart skins capable of on-demand dynamic texture morphing are attractive for several applications, ranging from haptic feedback devices^[1] to drag control in aerial or underwater vehicles.^[2] There are countless inspiring examples of biological creatures, which intelligently morph their skin patterns to achieve multifunctionality. For example, the leaves of the silver tree (*Leucadendron argenteum*) morph their hair-like texture

to survive throughout extreme hot dry or extremely humid weathers equally.^[3] A truly fascinating example of stretchable camouflaging texture morphing skin is seen in cephalopods—the underwater invertebrates known as the masters of camouflage. These marine creatures control their skin morphology by stimulating cutaneous muscles known as papillae. These muscles generate complex texture patterns by pushing the overlying epidermal tissue upward and away from the mantle surface during their contraction.^[4] Thanks to the large number of high-resolution texture muscles, cephalopods undergo complex morphology change. Overall, the skin of the cephalopod is a 3D display, where the papillae muscles control each voxel's extension on-demand by several millimeters out of the skin plane, create hierarchical textures, and collectively change the overall skin pattern. The generation of complex 3D shapes not only facilitates camouflage by pattern matching but also could enhance the swimming efficiency by controlling the hydrodynamic drag.

The material systems required to achieve such morphological changes are extremely heterogeneous and complex. The flexible and stretchable skin tissue of cephalopods is coupled to dermal shape-changing mechanisms, seamlessly embedded muscles, and integrated neurological sensing and control. A few texture and morphology change technologies inspired by cephalopods' papillae have been recently proposed. Wang et al.^[5] produce on-demand fluorescent patterns using electroactive and mechanoresponsive elastomers, where high electric voltage ($>50 \text{ kV mm}^{-1}$) induces surface roughness of a millimeter. Current material developments are underway to reduce the required voltage and increase the materials voltage breakdown strength of these materials. Pikul et al.^[6] use pneumatically actuated elastomeric membranes coupled to rigid mesh to achieve programmable 3D texture morphing. This material produces complex preprogrammed morphological camouflage, yet their broad applicability is limited by the need for heavy, rigid, and noisy air compressor.

In this study, we produce a new type of stretchable skin based on electromechanical digital texture voxels (DTV) to emulate the 3D morphing display of cephalopods papillae. The DTVs provide surface roughness, which actively changes its amplitude from the sub-millimeter to more than a centimeter and requires only 0.02 V mm^{-1} for actuation. These surface actuators undergo giant and reversible extensions exceeding 2000% strain within a few seconds. The DTVs are made from

Dr. C. Lamuta
Department of Mechanical Engineering
University of Iowa
Iowa City, IA 52242, USA
E-mail: caterina-lamuta@uiowa.edu

Dr. C. Lamuta, Prof. N. Sottos, Dr. S. Tawfick
Beckman Institute for Advanced Science and Technologies
University of Illinois at Urbana-Champaign
Urbana, IL 61801, USA
E-mail: tawfick@illinois.edu

H. He
Department of Electrical and Computer Engineering
University of Illinois at Urbana-Champaign
Urbana, IL 61801, USA

K. Zhang, M. Rogalski, Dr. S. Tawfick
Department of Mechanical Science and Engineering
University of Illinois at Urbana-Champaign
Urbana, IL 61801, USA

Prof. N. Sottos
Department of Material Science and Engineering
University of Illinois at Urbana-Champaign
Urbana, IL 61801, USA

 The ORCID identification number(s) for the author(s) of this article can be found under <https://doi.org/10.1002/admt.201900260>.

DOI: 10.1002/admt.201900260

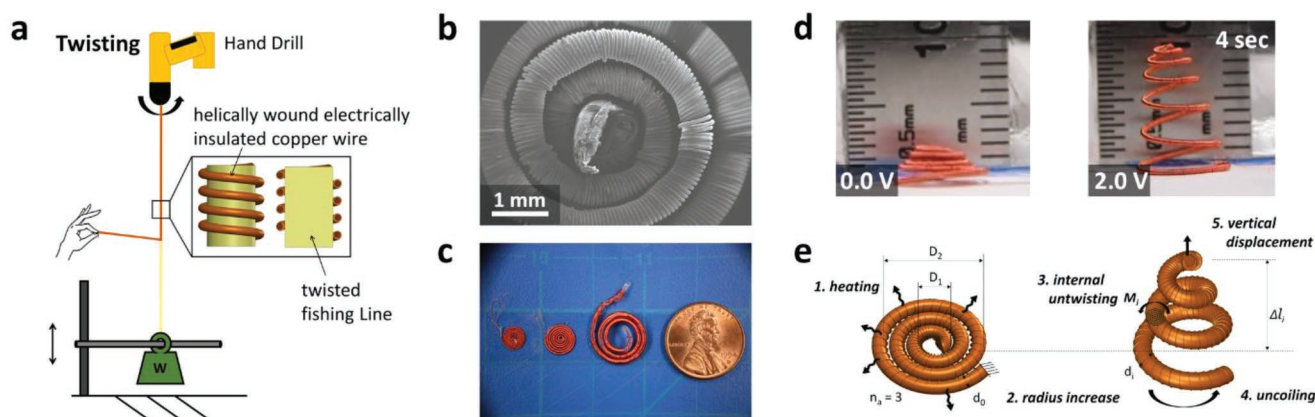


Figure 1. Twisted spiral artificial muscles (TSAM). a) Twisting of the polymer fiber and helical winding of copper wire; b) scanning electron microscopy image of a TSAM at the end of the manufacturing process; c) optical photographs of TSAMs produced using fishing lines with fiber diameter equal to 0.1, 0.3, and 1 mm (starting from the left), where the US penny having 19 mm diameter is used as a scale bar; d) optical photographs of the TSAM produced from PVDF before and after electrical actuation with an input voltage of 2 V for 4 s; and e) schematic representation of the actuation mechanism of TSAM from a flat Archimedean spiral to a conical helix. Enumerated steps denote the transduction mechanism due to joule heating.

inexpensive, commercially available polymer fishing line, which is twisted into flat Archimedean spirals. A flexible smart skin able to perform dynamic texture morphing is developed by attaching DTVs onto its surface. Further, by embedding DTVs within an elastomeric thin film, a shape-changing free standing skin is demonstrated. Since the DTVs can be individually addressed, this smart skin affords unlimited number of complex target skin patterns (Video S1, Supporting Information).

Twisted and coiled fibers are a new class of simple artificial muscles capable of exerting large contractile strains.^[7] These lightweight muscles can substitute traditional bulky electromagnetic actuators in applications where low weight, high contractile work, and fine motion are required. The fibers can be made from carbon nanotubes (CNTs) with a paraffin wax matrix,^[8] from polymer fibers such as nylon fishing line,^[9] from carbon fibers embedded in a silicone matrix,^[10] or from two-way shape memory polymer fibers.^[11] In particular, our recently developed carbon fiber coiled muscles are attractive since they can be actuated by joule heating or chemical swelling, lift 12 600 times their own weight by supporting up to 60 MPa of mechanical stress. They provide tensile strokes up to 60%, and a specific work up to 758 J kg⁻¹ (the latter is more than 18 times higher than that of natural muscles).^[10]

We use twisted spiral artificial muscles (TSAM pronounced as *Tee-Sam*) as individual DTVs for morphing skins (Figure 1). Figures 1a shows the new manufacturing process which is key to the realization of the TSAMs. Various types of fishing line, typically having 300 μm diameter, can be used to fabricate the TSAMs. A new fabrication process enables the simultaneous twisting of the fishing line and the winding of a thin copper wire around it for electrothermal actuation. The upper extremity of the polymer fiber is fixed in the chuck of a drill bit while a load is attached to its lower extremity and constrains the twisting of the bottom. The upper end of the copper wire is fixed to the side of the rotating chuck and the other end is slowly guided toward the polymer fiber as the drill twists it. As a result, the fishing line is twisted by the rotation of the drill, while the copper wire is helically wound around it. The details

of this fabrication process are further described in the Supporting Information. Notably, the resulting twisted polymer fiber is stable due to the copper wire winding. The twisted polymer-copper fiber is then shaped into a flat Archimedean spiral on an adhesive substrate that maintains the flat spiral geometry. Thermomechanical treatment sets the shape of the spiral polymer fiber-copper wire composite. A load is placed on the top of the sample while it is annealed in the oven at 135 °C for 2 h. The final configuration of a TSAM after coiling is shown in the scanning electron microscopy image in Figure 1b. Figure 1c showcases the ability of this simple manufacturing process to make a variety of spirals having different sizes. For instance, spirals having 5, 8, and 12 mm outer diameter are fabricated from commercial fishing lines having diameter of 0.1, 0.3, and 1 mm, respectively. Fishing lines with a diameter of 0.3 mm are selected for the development of DTVs as they provide high output force device with small voxel footprint. Figure 1d shows the electromechanical actuation of a single TSAM produced using polyvinylidene difluoride (PVDF) fishing lines. A voltage of only 2 V transforms the flat spiral into a helical cone within 4 s, where the vertical displacement of the tip is close to 1 cm. The flat spiral has a thickness equal to the fishing line/helical copper thickness of 0.44 mm, which when actuated becomes 9 mm, corresponding to a giant strain of 2045%. Considering the total length of the sample of 78 mm, the TSAM requires only 0.02 V mm⁻¹ to be actuated. This specific voltage value is considerably lower than the 54 kV mm⁻¹ required by texture modulations solutions based on electroactive elastomers.^[5]

The actuation mechanism of the TSAM is schematically shown in Figure 1e. The kinematics of TSAMs is reminiscent of telescoping helical conical springs with an initial flat configuration. TSAMs critically differ from conical springs by their internal twisted wire, which enables their actuation by releasing this stored torsional strain energy. When a current heats the TSAM, the twisted wire undergoes coupled diameter increase and local untwisting, which cause an overall uncoiling. The kinematics of the latter transforms a flat spiral into a vertical helical cone. The displacement of the cone tip is hence a function

of the inner and outer diameters and the number of turns and can reach heights approximately equal to the outer diameter. The parameters defining the initial geometry of the spring are illustrated on the left of Figure 1e: d_0 is the initial diameter of the twisted fiber, D_1 is the mean diameter of the smallest active coil, D_2 is the mean diameter of the largest active coil, and n_a is the total number of active spiral coils. Joule heating causes a simultaneous anisotropic expansion of the wire—increase in diameter only and not the length—and internal untwisting. The diameter increases from d_0 to d_i while its total length remains constant or slightly decreases.^[7] The anisotropic volume expansion (i.e., the mismatch between radial and axial expansion) causes an internal untwisting of the fiber (M_i moment in Figure 1e) which generates an external uncoiling of the spring and a vertical displacement Δl_i . Due to this specific mechanism, twisted and coiled artificial muscles (regardless of the shape, which can be helical or spiral) offer high performance owing to their anisotropic thermal expansion properties and the coupling of diametric expansion and untwisting, as achieved by CNTs,^[8] carbon fibers,^[10] or specific polymer fibers such as nylon, PVDF, or polyethylene.^[9] When the actuation mechanism originates from thermal expansion, its reversibility is guaranteed by the cooling stage. During cooling, the diameter of the twisted fibers returns to its original value and the artificial muscle recovers its internal twisting and original shape. However, the actuation is no longer reversible if the thermal degradation of the materials used for the TSAMs fabrication is reached. In particular, a thermal degradation of the polymer fibers used in this study (characterized by an initial diameter of 0.3 mm) is observed when the applied voltage is higher than 2 V, as shown in Figure S2 in the Supporting Information.

A theoretical model can guide the design of the load-displacement characteristics of the TSAMs. The coupling between the local diametric expansion (d_0/d_i) and the local untwisting moment M_i can be expressed by Equation (1) which is based on single helix theory^[12]

$$M_i = \frac{\pi d_i^4 G n_0}{32l} \left(1 - \frac{d_0}{d_i}\right) \quad (1)$$

where G is the shear modulus of the polymer fiber, n_0/l is the total number of turns per length applied during the initial twisting procedure, and $l = (\pi n_a/2)(D_1 + D_2)$ is the total length of a straight twisted fiber. The copper wire does not contribute to the mechanics as demonstrated by the analysis in the Supporting Information. The mechanics of TSAMs is similar to that of compression conical springs.^[13] In telescoping compression conical springs, the compression load causes an internal twisting and deflects the spring until reaching the ground configuration. The TSAMs have instead a ground configuration before actuation. The internal untwisting (due to diameter expansion) generates a tensile load extending the spring vertically. In telescoping compression conical springs, the relationship between the axial load and the deflection is usually considered linear until the first active coil reaches the ground and ceases to be an active element. The first contact with the ground defines the transition from a linear to a nonlinear behavior.^[14] For simple helical springs or solid conical springs, the nonlinearity is reached when adjacent active coils come into

contact.^[13] Since the TSAMs experience an elongation during actuation, they are not affected by the nonlinearity induced by coil–coil or coil–ground contact, and the relationship between the tensile local moment M_i and the vertical displacement Δl_i can be considered entirely linear. In the case of TSAM, the untwisting actuation moment M_i acts in the opposite direction to the moment resulting from the external load. Assuming that the actuated TSAM is a conical spring with constant pitch, its extension simplifies to (more details are in the Supporting Information)

$$\Delta l_i = \frac{(D_1^2 + D_2^2)n_0}{4D_2K_w} \left(1 - \frac{d_0}{d_i}\right) \quad (2)$$

where K_w is the Wahl curvature correction constant, which takes into consideration the spring index—the ratio between the wire and spiral diameter (additional details about the derivation of Equation (2) are provided in the Supporting Information). The final actuation of TSAMs with a specific geometry (i.e., D_1 and D_2) depends only on two factors: the inserted twist (i.e., n_0) and the fiber diameter expansion (i.e., d_0/d_i). A higher number of turns applied during twisting stores more energy inside the fiber, which can be released during heating-induced untwisting. Similarly, larger displacements can be obtained for materials having larger thermal expansion coefficient manifested as d_0/d_i . To confirm these insights, we compare the linear expansion of several TSAMs having various inserted twist turns. Figure 2a shows how the output displacement increases for increasing number of turns inserted during twisting in TSAMs produced using PVDF fishing lines with an initial diameter $d_0 = 0.3$ mm, final diameter $d_i = 0.39$ mm (measured under a microscope during Joule heating), $D_1 = 3.8$ mm, $D_2 = 11.5$ mm, and $n_a = 5$. The good agreement between experimental results and theoretical predictions (obtained using Equation (2)) confirms the suitability of the proposed model to describe the actuation mechanism and the performance of TSAMs. This linear trend between the number of turns and the resulting displacement shows the role of geometric strain amplifications, making the DTV uniquely attractive. The initial number of turns represents the strain energy stored in the coils during fabrication, which can be released on-demand during operation simply by heating.

The performance of the TSAMs under compression load W can also be calculated using the theoretical model proposed herein. The vertical displacement under external load Δl_{iw} is obtained as follows

$$\Delta l_{iw} = \Delta l_i - \frac{2n_a(D_1^2 + D_2^2)(D_1 + D_2)}{Gd_i^4} W \quad (3)$$

The displacement under load, Δl_{iw} , depends on the number of inserted turns through Δl_i . Figure 2b shows how the vertical displacement provided by TSAMs decreases for increasing values of the applied compression load W . Three different types of polymer fibers are tested, nylon monofilament (labeled as “Mono” in Figure 2b), PVDF monofilament (labeled as “Fluoro”), and braided polyethylene fibers (labeled as “Braided”). These samples are tested under the same heating conditions (an input voltage of 2 V was applied for 4 s). The final diameter at this applied voltage/time is $d_i = 0.39$ mm as

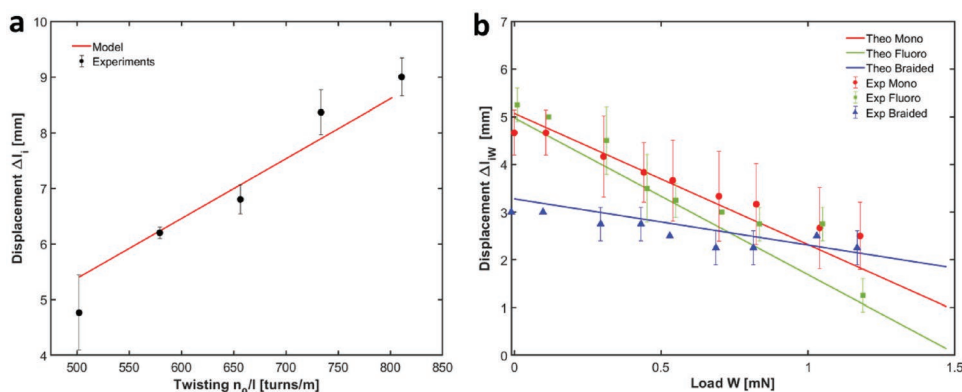


Figure 2. Performance of the TSAMs. a) Output displacement versus inserted number of turns for TSAMs produced using PVDF fibers with a shear modulus $G = 0.34$ GPa (calculated as $G = E/2(1 + \nu)$, where $E = 0.921$ GPa^[15] and $\nu = 0.348$ ^[16]), an initial diameter $d_0 = 0.3$ mm, $D_1 = 3.8$ mm, and $D_2 = 11.5$ mm, $n_a = 5$. Three samples for each number of turns were tested. The average value and standard deviation of the output displacement are reported. An input voltage equal to 2 V is applied for 4 s in order to actuate the TSAMs. Theoretical results were obtained using Equation (2) and the value of the final diameter $d_i = 0.39$ mm. b) Output displacement versus applied compression load for TSAMs produced using three different types of fishing lines: “SpiderWire EZ Mono” nylon monofilaments (indicated as “Mono”), “SpiderWire EZ Fluoro” PVDF monofilaments (indicated as “Fluoro”), and “SpiderWire EZ Braided” polyethylene braided fibers (indicated as “Braided”). An input voltage equal to 2 V was applied for 4 s in order to induce Joule heating. All the samples are produced using an inserted twist of $n_0/l = 800$ turns m^{-1} and have $n_a = 5$, an initial diameter $d_0 = 0.3$ mm, and a final diameter $d_i = 0.39$ mm (since the three materials have almost identical coefficient of radial thermal expansion, between 5×10^{-6} and 7×10^{-6} K^{-1} ,^[17] the same input voltage leads to a similar radius increase). Three samples for each applied load are tested and mean values of D_1 and D_2 are considered for the three types of artificial muscles. The values used in the linear model are $D_1 = 3$ mm and $D_2 = 9$ mm for the nylon samples, $D_1 = 3$ mm and $D_2 = 8.8$ mm for the PVDF samples, $D_1 = 1.4$ mm and $D_2 = 6.28$ mm for the braided polyethylene samples. A shear modulus G of 0.43,^[12] 0.34 GPa (calculated as $G = E/2(1 + \nu)$, where $E = 0.921$ GPa^[15] and $\nu = 0.348$ ^[16]), and 0.36 GPa (calculated as $G = E/2(1 + \nu)$, where $E = 1.002$ GPa^[18] and $\nu = 0.41$ ^[19]) was considered for nylon monofilaments, PVDF monofilaments, and polyethylene braided fibers, respectively. The average value and standard deviation of the output displacement are reported. Theoretical results were obtained using Equation (3).

measured under an optical microscope. The three types of fishing line undergo a linear decrease in vertical displacement actuation with the increase of applied load and a good agreement between experimental data and theoretical prediction is observed. The theoretical curves shown in Figure 2b are calculated using the experimental values of $d_0 = 0.3$ mm, $n_a = 5$, and $n_0/l = 800$ turns m^{-1} . We observe that samples of different materials show a slightly different actuation behavior. This difference is related to the different equilibrium geometrical configurations reached by the different materials after the thermo-mechanical annealing process. While all samples are shaped to the same value of D_1 and D_2 (Figure 1b), the annealing step results in a slightly different D_1 and D_2 . While the braided polyethylene samples maintain the imposed spiral geometry to a large fidelity, nylon and PVDF samples experience a slight 2D expansion leading to larger values of D_1 and D_2 . This expansion causes a higher initial displacement at zero compression load (Δl_i is the starting point of the Δl_{iW} vs W curves and it is related to D_1 and D_2 according to Equation (2)) and a faster decrease of the output displacement for increasing values of the compression load W (the slope of the Δl_{iW} vs W curve is related to D_1 and D_2 according to Equation (3)). Equations (2) and (3) are very useful to tailor the geometry of TSAMs according to the target output displacement under specific loading conditions.

The displacement values reported in Figure 2 are obtained by applying low voltages for short durations to prevent heat-induced degradation and maintain the reversible actuation of the TSAMs. Higher values lead to temperatures higher than 65 °C (see Figure S2, Supporting Information) and to the thermal degradation of the polymer fibers which causes

irreversible untwisting. Notably, the value of the work density obtained from the tested TSAMs is equal to 0.115 J kg^{-1} . This value is significantly lower than that measured for fishing line twisted and coiled artificial muscles (TCAMs) with a helical shape, working in the common contraction configuration (i.e., 2500 J kg^{-1}).^[9] This difference is related to the number of turns inserted during fabrication, as well as the spring index value. The number of turns per meter represents the stored elastic strain energy in any twisted artificial muscle, and larger stored energy leads to larger work density. An inserted twist of 3020 turns m^{-1} is applied to helical TCAMs,^[9] while a value of 800 turns m^{-1} is used for the TSAMs produced herein. The maximum numbers of turns inserted in TSAMs is always lower than that of helical TCAMs to avoid spontaneous coiling. When the spring index increases the stiffness of the helical decreases, as well as its ability to sustain high mechanical loads. The highest value of work density in helical TCAMs is measured for spring index values (i.e., coil diameter/fiber diameter ratio) close to 1.^[9] Due to the spiral shape, the spring index of the TSAMs is usually much bigger than 1 (the spring index for the samples produced in this study is > 30), and this leads to a significant decrease of force generation and work density (see Equation (S10) in the Supporting Information). Due to the low value of the output force provided by the TSAMs produced in this study (in the range of a few milliNewtons, as shown in Figure 2b), a low value of efficiency, equal to 0.00064%, is recorded. The efficiency is calculated as the ratio between the output mechanical energy and the input electrical energy, according to the following equation: $\eta = (W \Delta l_{iW}) / (V I t)$, where W is the maximum output force provided, Δl_{iW} is the

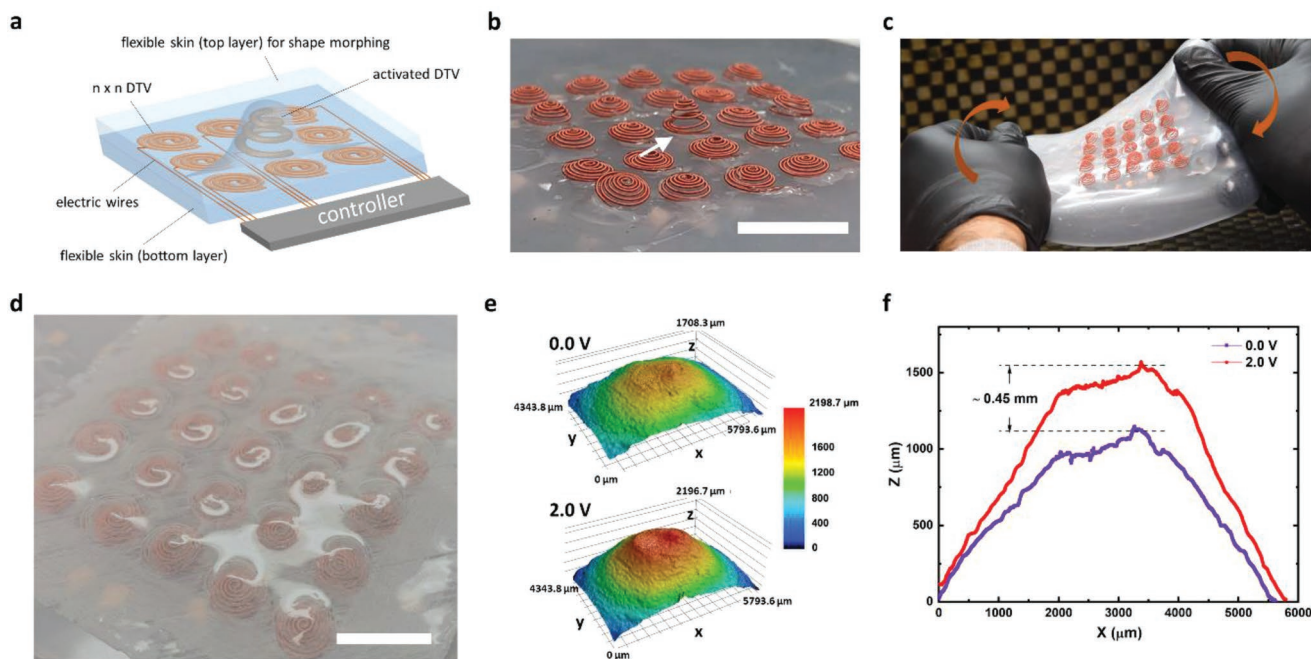


Figure 3. Stretchable morphing skin from DTV. a) Schematic representation of the final device for digital texture morphing where $n \times n$ TSAM are attached to a bottom silicone layer. Each TSAM is electrically connected to a microcontroller by means of electric wires and referred to as a DTV. A silicone top layer is deposited to the TSAMs matrix to achieve shape modulation; b) optical photograph of the artificial skin for texture morphing where the actuation of the central DTV is shown; c) Demonstration of flexibility of the artificial morphing skin (see video in the Supporting Information); d) optical photograph of the artificial skin for shape morphing where a top silicone layer is added to cover the DTVs. This top layer couples the mechanicals of the skin to the motion of the TSAMs to cause shape morphing; e) 3D profiles of a covered DTV before (0.0 V on the top) and after (2.0 V below) actuation, obtained by optical profilometry (Keyence 3D laser scanning microscope VK-X1000); f) vertical position (Z) of the embedded DTV measured along its central cross-section before (0.0 V) and after (2.0 V) actuation. All scale bars are 20 mm.

vertical displacement, V is the applied voltage, and I is the current applied for a certain time t . The low efficiency is one of the main drawbacks of thermally and electro-thermally actuated artificial muscles due to heat loss in free convection conditions.^[7] The maximum efficiency measured for electro-thermally actuated twisted and coiled artificial muscles with a helical shape is in the range of 1%.^[10] TSAMs show lower efficiency compared to twisted and coiled artificial muscles with a simple helical shape due to their higher spring index which leads to lower stiffness and output force. However, we do not believe that this is practically a problem as these actuator can only be used for very small values of mechanical work. Nonetheless, the use of different materials (e.g., materials with a higher coefficient of thermal expansion and/or a higher electrical resistance that requires lower temperature and/or electric voltage for volume expansion), or different convection conditions, can potentially lead to an increase of the TSAMs efficiency.

A stretchable skin device for texture morphing is produced in order to demonstrate the suitability of TSAMs to perform as DTVs. The device is shown in **Figure 3**. A 5×5 matrix of TSAMs is placed on a flexible elastomer substrate having 3 mm thickness (Smooth-On Ecoflex 00–30). A small amount of uncured elastomer is used to fix the outer coil of each TSAM to the substrate. The two extremities of the thin copper wire wrapped around each fishing line are transferred to the back side of the substrate, and then soldered to thicker

copper wires and connected to the pins of a microcontroller for electrical actuation, as shown in **Figure 3a**. Each TSAM can be individually controlled to produce different output texture patterns. We have also demonstrated covering the DTVs by an additional elastomeric top layer. **Figure 3b** shows an example of texture morphing where only a single DTV at the center of the 5×5 array is actuated, while **Figure 3d** shows the device with a 200 μm thick elastomeric top layer. In order to reduce the friction between the TSAMs and the top layer during actuation, we created recessed patterns in the top layer by spin coating the layer onto a mold having the required features (more information can be found in **Figure S3** in the Supporting Information). As shown in **Figure 3e,f**, the devices can still actuate in the presence of the top layer by stretching it vertically. We measure the profile of the displacement using 3D laser scanning microscopy. The maximum displacement for an embedded DTV actuated with an electrical input of 2 V is equal to 0.45 mm. While this is a large decrease from the 10 mm displacement of the uncovered DTV (**Figure 1d**), it is still an outstanding vertical strain of nearly 100%. Further, future optimization of the elastomer cover geometry could lead to increased strain, such as by the incorporation of small local wrinkles. Currently, the actuation of the TSAM is causing the stretching of the elastomer. **Movie S1** in the Supporting Information demonstrates the texture morphing capabilities with different complex output patterns with and without the elastomer cover. Notably, this flexible artificial skin can be

manipulated, stretched and twisted during the operation of the DTVs without affecting the performance. This performance can be attributed to the structural flexibility of the spiral-shaped DTVs. Figure 3c (snapshots from Movie S1, Supporting Information) shows the flexibility of the skin under various manipulations.

The final device is a soft and flexible smart skin, where TSAMs act as DTVs and can be individually activated to produce dynamic texture morphing waves. The maximum roughness of the output texture (i.e., the maximum displacements performed by TSAMs) is tailored by choosing the geometry of the TSAMs according to Equations (2) and (3). Once the maximum output height is fixed, the instantaneous height of each DTV is controlled by the input voltage. Notably, the device response time (<5 s) is much faster than pneumatic artificial texture skins. Performance of the skin can be further increased by designing the appropriate circuit elements to drive the required joule heating currents within less than a second.

Thanks to the ability of the DTV to provide on-demand textures and patterns, the flexible and lightweight artificial skin demonstrated herein will potentially surpass the ability of biological systems in texture morphing, and pave the way for innovative applications beyond camouflage, such as visual 3D displays, Braille displays, temperature and light responsive skins, and fouling resistant surfaces ranging from ship hulls to biomedical devices.

Supporting Information

Supporting Information is available from the Wiley Online Library or from the author.

Acknowledgements

C.L. acknowledges support by the Postdoctoral Fellowship of the Beckman Institute for Advanced Science and Technologies at the University of Illinois Urbana-Champaign and by the Office of Naval Research N00014-19-1-2136. S.T., H.H., M.R. were supported in part by the National Science Foundation CMMI 18-25758 and by the Air Force AF FA9550-19-1-0010.

Conflict of Interest

The authors declare no conflict of interest.

Keywords

digital voxels, soft skin, texture morphing, twisted spiral artificial muscles

Received: March 26, 2019

Revised: May 2, 2019

Published online: May 29, 2019

- [1] C. Pacchierotti, S. Sinclair, M. Solazzi, A. Frisoli, V. Hayward, D. Prattichizzo, *IEEE Trans. Haptics* **2017**, *10*, 580.
- [2] S. Daynes, P. M. Weaver, *Proc. Inst. Mech. Eng., Part D* **2013**, *227*, 1603.
- [3] a) B. Bhushan, *Philos. Trans. R. Soc., A* **2009**, *367*, 1445; b) C. A. Brewer, W. K. Smith, T. C. Vogelmann, *Plant, Cell Environ.* **1991**, *14*, 955.
- [4] a) J. J. Allen, G. R. Bell, A. M. Kuzirian, R. T. Hanlon, *J. Morphol.* **2013**, *274*, 645; b) P. T. Gonzalez-Bellido, A. T. Scaros, R. T. Hanlon, T. J. Wardill, *iScience* **2018**, *2*, 101.
- [5] Q. Wang, G. R. Gossweiler, S. L. Craig, X. Zhao, *Nat. Commun.* **2014**, *5*, 4899.
- [6] J. H. Pikul, S. Li, H. Bai, R. T. Hanlon, I. Cohen, R. F. Shepherd, *Science* **2017**, *358*, 210.
- [7] C. S. Haines, N. Li, G. M. Spinks, A. E. Aliev, J. T. Di, R. H. Baughman, *Proc. Natl. Acad. Sci. U. S. A.* **2016**, *113*, 11709.
- [8] M. D. Lima, N. Li, M. J. de Andrade, S. L. Fang, J. Oh, G. M. Spinks, M. E. Kozlov, C. S. Haines, D. Suh, J. Foroughi, S. J. Kim, Y. S. Chen, T. Ware, M. K. Shin, L. D. Machado, A. F. Fonseca, J. D. W. Madden, W. E. Voit, D. S. Galvao, R. H. Baughman, *Science* **2012**, *338*, 928.
- [9] C. S. Haines, M. D. Lima, N. Li, G. M. Spinks, J. Foroughi, J. D. W. Madden, S. H. Kim, S. L. Fang, M. J. de Andrade, F. Goktepe, O. Goktepe, S. M. Mirvakili, S. Naficy, X. Lepro, J. Y. Oh, M. E. Kozlov, S. J. Kim, X. R. Xu, B. J. Swedlove, G. G. Wallace, R. H. Baughman, *Science* **2014**, *343*, 868.
- [10] C. Lamuta, S. Messelot, S. Tawfick, *Smart Mater. Struct.* **2018**, *27*, 055018.
- [11] Q. Yang, J. Fan, G. Li, *Appl. Phys. Lett.* **2016**, *109*, 183701.
- [12] S. Aziz, J. Foroughi, H. R. Brown, G. M. Spinks, *J. Polym. Sci., Part B: Polym. Phys.* **2016**, *54*, 1278.
- [13] A. M. Whal, *Mechanical Springs*, McGraw-Hill Book Company, New York **1963**.
- [14] E. Rodriguez, M. Paredes, M. Sartor, *J. Mech. Des.* **2006**, *128*, 1352.
- [15] A. Ferreira, P. Costa, H. Carvalho, J. M. Nóbrega, V. Sencadas, S. Lanceros-Mendez, *J. Polym. Res.* **2011**, *18*, 1653.
- [16] A. Vinogradov, F. Holloway, *Ferroelectrics* **1999**, *226*, 169.
- [17] R. A. Orwoll, in *Physical Properties of Polymers Handbook*, (Ed: J. E. Mark), Springer, New York **2007**, Ch. 7.
- [18] I. M. G. Bertelsen, L. M. Ottosen, presented at *Int. RILEM Conf. on Materials, Systems and Structures in Civil Engineering*, Technical University of Denmark, Lyngby, Denmark, August **2016**.
- [19] F. Addiego, A. Dahoun, C. G'Sell, J.-M. Hiver, *Polymer* **2006**, *47*, 4387.